DOI: 10.21917/ijivp.2023.0440

ACCURATE MOTION ESTIMATION FOR ROTATIONAL IMAGE SEQUENCES

Hirak Doshi and N. Uday Kiran

Department of Mathematics and Computer Science, Sri Sathya Sai Institute of Higher Learning, India

Abstract

Complex motion patterns, non-rigid deformations, occlusions, and illumination changes largely affect rotational image sequences. This makes accurate motion estimation a challenging task. To address this issue, we propose an optical flow model to accurately estimate motion in rotational image sequences. Our model uses an additional constraint in the objective weighted with an edge-stopping function which allows non-zero curl specifically in the regions where rotation is involved. Our implementation of the model relies upon the robust Chambolle-Pock algorithm. We discuss the effects of the model parameters and the primal-dual parameters in the convergence of the algorithm. To further validate the effectiveness of our model, we combine our algorithm with some of the sophisticated implementation approaches with weighted median filtering. Our results on some of the rotational sequences from the Middlebury benchmark datasets show that our method achieves the best average angular and end-point errors when compared with some of the well-known models in the literature.

Keywords:

Motion Estimation, Primal-Dual, Rotational Motion

1. INTRODUCTION

Optical flow estimation is the process of estimating the motion of objects in a sequence of images or video frames. It is an important and challenging problem in computer vision with many applications in robotics, autonomous vehicles and video processing.

The basic idea behind optical flow estimation is to track the movement of pixels from one frame to the next and then use this information to estimate the velocity field of the scene. This is typically done by computing the displacement of pixels between two adjacent frames and then applying some optimization techniques to estimate the underlying flow field.

Accurate motion estimation in image sequences is often a difficult problem that involves many factors.

a. *Illumination changes*: Illumination changes such as variations in lighting or shadowing can cause significant changes in the appearance of objects in the scene. These changes can make it difficult to track the motion of objects accurately.

b. *Large displacements*: When there is a large displacement between frames, the motion estimation problem becomes more challenging as the underlying motion assumptions become invalid.

c. *Occlusions*: Occlusions occur when one object in the scene blocks the view of another object. This leads to errors in motion estimation as the motion of the occluded object cannot be directly observed.

d. *Motion boundaries*: The motion boundaries between objects in the scene can be difficult to detect and track accurately. These boundaries are often regions of high contrast in the images.

1.1 RELATED WORK

Several methods have shown promising solutions to deal with the challenges discussed above. Variational methods have been shown to be effective for optical flow estimation in many applications and have been extended to handle various types of image data and different types of motion, including occlusions and discontinuities.

The approach of the Horn-Schunck method [1] assumes that the motion between frames is smooth and continuous. While this algorithm is widely used and has many strengths, it also has some drawbacks which involve global smoothness assumptions, sensitivity to noise, difficulty in handling discontinuities and so on.

Several models have suggested improvements over the Horn and Schunck models. An early modification based on the total-variation (TV) regularization was suggested by Cohen [3]. Aubert et al. [2] formulated a new discontinuity-preserving model under a rigorous mathematical foundation. An improved algorithm for *TV-L*^{1} optical flow was proposed in [4]. Several optical flow models were analyzed in [5].

The accuracy of optical flow models has significantly improved over the years, as a result of advancements in optimization techniques and better evaluation metrics. Some of the remarkable contributions for obtaining high accuracy optical flow algorithms are due to [7,8,14]. A performance evaluation of several optical flow models can be found in [6].

1.2 OUR CONTRIBUTIONS

Our main goal is to develop an accurate motion estimation scheme for rotational image sequences. In this context, we propose a model comprising of the optical flow constraint as a quadratic minimization with the total-variation (TV) regularization term. There is an additional constraint term introduced in the model for capturing the rotational motion in the flow. This term penalizes the curl of the flow weighted with an anisotropic edge-stopping function. This constraint term encourages the flow to have zero curl in the regions of the image where there is no rotational motion, and allows for non-zero curl in regions where there is rotational motion.

We employ the Chambolle-Pock [10] primal-dual algorithm for the numerical implementation of our model which is highly robust and can be adapted to solve a wide class of non-smooth convex optimization problems. We discuss in detail the influence of model parameters and the primal-dual parameters in achieving the desired convergence.

To further improve the flow accuracy, we combine the numerical scheme with sophisticated implementation approaches which significantly contribute towards improving the average angular and end-point errors. Here a detailed discussion of the weighted median filtering and its effectiveness is presented.

The proposed approach has relevance in important application domains like cardiac motion estimation where one can capture the vortices of the blood flow within the valve accurately. Further, our model can handle illumination variations in challenging image sequences such as Jupiter's white oval sequence [19, 20]. On this dataset, we have shown in one of our works how a flow-driven refinement process involving the curl of the flow can actually outperform rotational-based in particular and classical physics-based refinement techniques in general without any additional assumptions on the image data.

The organization of the paper is as follows. In Section 2, we give a description of our proposed model. In Section 3, we discuss the numerical implementation of our model using the primal-dual algorithm. Here we show our results on some rotational image sequences and also discuss the selection of parameters for the convergence of the algorithm. Subsequently, in Section 4, we discuss techniques that have led to improvements in flow estimation. Here we discuss in detail the weighted median filtering and also the appropriate choice of parameters. We show our results on some rotational image sequences from the Middlebury benchmark datasets and compare our results with some of the well-known variational optical flow models.

2. PROPOSED MODEL

Based on the above discussion, we propose the following model:

$$\min_{u} \left\| f_t + \nabla f \cdot u \right\|_2 + \alpha \sum_{i=1}^{2} \left\| \nabla u_i \right\|_1 + \beta \left\| \nabla_o \cdot u \right\|_{\phi,2} \tag{1}$$

where $\boldsymbol{u}$ is the optical flow, Ω is an open and bounded subset of R^2, α, β are model parameters, $\|\cdot\|_2 = \sum_\Omega |\cdot|^2$ is the quadratic L^2 norm, $\|\cdot\|_1$ is the standard 1-norm, the operator $\nabla_o=(\partial y,-\partial x)$ denotes the 2D curl operator.

The model has three terms. The first term is the standard quadratic penalization of the optical flow constraint. The second term is the total variation minimization of the flow components which encourages smoothness in regions where the flow is spatially consistent while allowing for discontinuities at edges and other regions of high spatial variation. This can help to avoid over-smoothing of the flow field and preserve important spatial features.

The third term is a special constraint term defined as:

$$\left\| \nabla_o \cdot u \right\|_{\phi,2} := \sum_{\Omega} \phi\left(\left| \nabla f \right| \right) \left(\nabla_o \cdot u \right)^2 \tag{2}$$

The presence of a vortex in the fluid indicates rotation around an axis. In such regions, the vectors change the direction along different paths around the point. A higher curl value indicates a rapid change in the direction of velocity vectors. Whether the rotation is clockwise or counterclockwise is known from the curl being negative or positive.

The edge-stopping function ϕ is used as a weight term on the curl of the flow in the constraint term of the model. This is done to give higher weightage to the rotational components of the flow which are known to have a curl. The edge-stopping function acts as a regularizer ensuring that the constraint term penalizes only the rotational components of the flow and not the translational ones.

The edge-stopping function is typically derived from the gradient magnitude of the input image. It assigns higher weightage to regions of the image with strong edges and lower weightage to regions with weak edges or no edges. This ensures that the constraint term gives more importance to the rotational flow components in regions with strong edges where the rotational features are more likely to occur.

For the current work, we use the edge-stopping function as highlighted by Perona and Malik [11]:

$$\phi\left(\left| \nabla f \right| \right) = \frac{K^2}{K^2 + \left| \nabla f \right|^2} \tag{3}$$

By using the edge stopping function as a weight term on the curl of the flow, the constraint term of the model is able to capture the rotational features of the flow more accurately. This leads to better estimates of the optical flow, especially in regions with strong rotational features such as vortices or swirling motion.

3. NUMERICAL IMPLEMENTATION

3.1 THE PRIMAL-DUAL ALGORITHM

Given a primal problem of the form,

$$\arg\min_{u} P_1(u) + P_2(Ru) \tag{3}$$

The primal-dual formulation is given as:

$$\arg\min_{u} \arg\max_{d} P_1(u) + P_2(Ru, d) - P_2^*(d) \tag{4}$$

where $u=(u_1,u_2)$, $d=(d_1,d_2,d_3)$ are the primal and dual variables respectively, P_1 corresponds to the data term of the model, P_2 relates to the regularization term, R is a differential operator governing certain intrinsic flow characteristics. P_2^* is the convex conjugate of P_2. The Chambolle-Pock algorithm solves the primal-dual problem using the following algorithm:

$$d^{k+1} = prox_{\sigma P_2^*}\left(d^k + \sigma R \bar{u}^k \right) \tag{5}$$

$$u^{k+1} = prox_{\tau P_1}\left(u^k + \tau R^* d^{k+1} \right) \tag{6}$$

$$\bar{u}^{k+1} = u^{k+1} + \theta\left(u^{k+1} - u^k \right) \tag{7}$$

where,

$$prox_{\tau f}(x) = \left(1 + \tau \partial f\right)^{-1}(x) = \arg\min_{y} \left\{ \frac{1}{2}\|x - y\|^2 + \tau f(y) \right\} \tag{8}$$

is the proximal or resolvent operator. The operator tries to balance between minimizing f and being close to x. The parameter τ acts as a trade-off between them [6]. The last relation in the algorithm is an over-relaxation step with θ being the relaxation parameter valued between 0 and 1.

In our problem, these terms are given by:

$$P_1 = \left\| f_t + \nabla f \cdot u \right\|_2$$

$$P_2 = \beta \left\| \nabla_o \cdot u \right\|_{\phi,2} + \alpha \sum_{i=1}^{2} \left\| \nabla u_i \right\|_1 \tag{9}$$

The operator R is given as:

$$R = \begin{bmatrix} \nabla & 0 \\ 0 & \nabla \\ \phi\partial_x & \phi\partial_y \end{bmatrix} \tag{10}$$

The convex conjugate $F^*(d)$ is computed as:

$$P_2^* = \frac{1}{2\beta}\|d_3\|_2 + \alpha\sum_{i=1}^{2}\delta_{B(L^\infty)}\left(\frac{d_i}{\gamma}\right). \tag{11}$$

Thus, the primal-dual formulation is given as:

$$\begin{aligned}\arg\min_u \arg\max_d \|f_t + \nabla f \cdot u\|_2 + (u, R^* d) \\ -\frac{1}{2\beta}\|d_3\|_2 + \alpha\sum_{i=1}^{2}\delta_{B(L^\infty)}\left(\frac{d_i}{\gamma}\right)\end{aligned} \tag{12}$$

After deriving the optimality conditions, the modified Chambolle-Pock algorithm for the current problem is presented below.

Algorithm 1:

1. Define τ, σ.
2. Initialize $u^0 \leftarrow 0$, $d^0 \leftarrow 0$
3. Initialize matrix R
4. **repeat**
5. $u_{old} \leftarrow u$
6. $\tilde{d} = d + \sigma R\bar{u}$
7. $d_{1,2} = proj_{\sigma/x}\left(\tilde{d}_{1,2}\right)$
8. $d_3 = \frac{\beta}{\beta+\sigma}\left(\tilde{d}_3\right)$
9. Compute matrix R^*
10. $\tilde{u} = u - \tau R^* d$
11. $u = \left(\frac{b_1c_3 - c_2b_2}{c_1c_3 - c_2^2}, \frac{b_2c_1 - c_2b_1}{c_1c_3 - c_2^2}\right)$
12. $\tilde{u} = 2u - u_{old}$
13. **until convergence**

The dual update for $d_{1,2}$ can be obtained by the point-wise projection of $\tilde{d}_{1,2}$ onto [-α,α] (see [12,13]) given as:

$$d_{1,2} = proj_{\sigma/x}\left(\tilde{d}_{1,2}\right) = \min\left(\alpha, \max\left(-\alpha, \tilde{d}_{1,2}\right)\right) \tag{13}$$

The sub-problem for d_3 is a linear quadratic minimization problem which is easily computed. The primal update $\boldsymbol{u}$ is obtained by solving a linear quadratic optimization. The components of the flow indicated in step 11 of the algorithm are obtained as:

$$c_1 = 1+\tau f_x^2,\ c_2 = \tau f_x f_y,\ c_3 = 1+\tau f_y^2,\ b_1 = \tilde{u}_1^{k+1} - \tau f_x f_t,$$
$$b_2 = \tilde{u}_2^{k+1} - \tau f_y f_t.$$

Step 12 in the algorithm is an over-relaxation step corresponding to the choice θ=1 in the Chambolle-Pock algorithm, see [10].

3.2 RESULTS ON ROTATIONAL IMAGE SEQUENCES

In this section, we show the performance of our proposed model using the primal-dual algorithm on well-known rotational image datasets, specifically the oseen vortex pair and the cloud sequence, see [18] for more details. By analyzing the flow fields generated by our model, we observe that it is able to accurately capture the intricate vortex patterns present in these datasets.

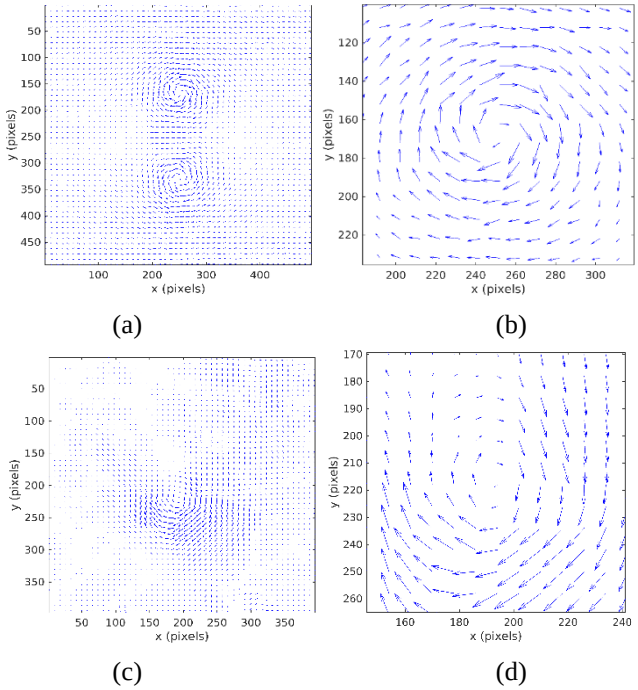

Fig.1. (a) Vorticity plot for the oseen vortex pair. (b) Close-up of the first vortex core of the oseen pair. (c) Vorticity plot for the cloud sequence. (d) Close-up of the main vortex core of the cloud sequence

The flow estimates produced by our model (Fig.1) exhibit smooth and consistent behavior. Furthermore, the results indicate that our model is robust and capable of handling complex rotational motion with a reliable degree of accuracy. Thus, the performance of our model on these datasets highlights its effectiveness in capturing the underlying flow patterns present in rotational image sequences.

3.3 SENSITIVITY OF FLOW TO PRIMAL-DUAL PARAMETERS

The primal and dual residuals are defined as:

$$p_r^{(k)} = \left|\frac{u_e}{\tau} - K^* d_e\right|, d_r^{(k)} = \left|\frac{d_e}{\sigma} - Ku_e\right| \tag{14}$$

where $u_e := u^k - u^{k+1}$, $d_e := d^k - d^{k+1}$ are the error between successive iterates for the primal and dual variables respectively.

The normalized residual error at the k^{th} iteration is then computed as:

$$e^{(k)} = \frac{p_r^{(k)} + d_r^{(k)}}{|\Omega|} \tag{15}$$

where $|\Omega|$ is the dimension of the domain Ω.

In our work, we have investigated the sensitivity of flow estimates to primal-dual parameters τ and σ respectively. Our observations demonstrate that the choice of these parameters plays a crucial role in the convergence of the algorithm.

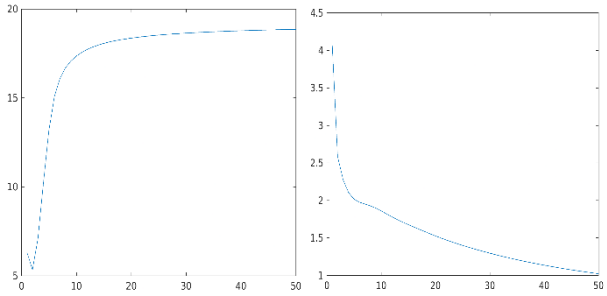

(a) (b)

Fig.2. (a) Residual flow error when τ=0.4 and σ=0.8. (b) Residual flow error when τ=0.4 and σ=0.25.

Specifically, we found that the flow estimates converge when $\tau>\sigma$, while the algorithm fails to converge when $\tau<\sigma$. This observation has direct implications on the design and implementation of primal-dual algorithms, as it highlights the importance of careful selection of primal-dual parameters to achieve convergence.

To illustrate this phenomenon, we conducted experiments by varying τ and σ between 0 and 1 and choosing a candidate set {0.1,0.25,0.4,0.6,0.8 and 1} of values for both parameters that satisfied the convergence criterion $\tau\sigma|K|^2<1$. We plotted the error between successive iterates for various combinations of τ and σ and found that the choice of parameters had a significant impact on the convergence of the algorithm. Two representative examples are presented in Fig.2, with (τ,σ)=(0.4,0.8) and (τ,σ)=(0.4,0.25), respectively, to demonstrate the differences in convergence behavior.

Our observation of the sensitivity of flow estimates to primal and dual parameters is a crucial consideration in the design of primal-dual algorithms. While the choice of these parameters depends on the specific problem and algorithm, the convergence condition we have observed provides a useful guideline. These results demonstrate the importance of choosing appropriate step sizes to achieve convergence in primal-dual optimization.

3.4 EFFECT OF MODEL PARAMETERS ON CONVERGENCE

In this section, we investigate the effect of model parameters α, β on the convergence of the flow for the cloud sequence and the oseen vortex pair.

For the cloud sequence, we observed that when $\tau>\sigma$, the algorithm converges when the ratio $\beta/\alpha\leq10^{-2}$. This indicates that the choice of β is not very critical and can be set to a relatively small value. However, it is important to choose α carefully as the algorithm does not converge if alpha is too small.

On the other hand, for the oseen vortex pair, we found that the choice of α is even more important for convergence. In addition to the above relation, we experimentally observed that the value of $\alpha \geq 0.4$ for the algorithm to converge. This suggests that α should be selected carefully, depending on the specific dataset being used.

In summary, our experiments suggest that the values of model parameters α and β, as well as the relationship between τ and σ, can have a significant impact on the convergence of the flow.

It is worth noting that the choice of model parameters also depends on the specific implementation of the algorithm. For example, the use of different numerical schemes or optimization methods may require different parameter values. Therefore, it is important to carefully tune the model parameters based on the specific implementation being used.

4. EFFECTIVE TECHNIQUES FOR IMPROVED FLOW ESTIMATION

4.1 ESSENTIAL IMPLEMENTATION APPROACHES

Modern implementation practices have proven highly effective in improving flow estimates and reducing angular errors on benchmark datasets [16] [17]. The success of these practices is largely attributed to several crucial intermediate optimization steps in the implementation scheme.

One such step involves the use of a coarse-to-fine grid, which has been shown to be effective in accounting for large pixel displacements. This technique entails computing incremental flow between the original image and the warped image obtained through bi-cubic interpolation using estimates from the coarse level. The incremental flow is computed between the original image and the warped image.

Moreover, the computation of image derivatives has been identified as another important intermediate step. This step is achieved using a standard five-point finite-difference stencil to estimate the derivative of the second image. The estimate is then warped towards the derivative of the first image, and an average of the derivative of the first image with the warped derivative is computed [7]. This technique has been found to be effective in improving flow estimates and reducing errors.

4.2 WEIGHTED MEDIAN FILTERING

An important intermediate step in flow optimization is the application of median filters to remove outliers. However, there are certain drawbacks of standard median filtering. Firstly, it leads to higher energy solutions [9]. Secondly, it may fail to preserve important image details by discarding its temporal order information, see [21]. The weighted median filter is an extension of the traditional median filter where each pixel in the neighborhood is assigned a weight based on its similarity to the center pixel. The weights are computed using a kernel, which specifies the shape and size of the neighborhood around each pixel.

According to Li and Osher's formula [9] we have the following formula:

$$\sum_i \min_x w_i\left(x-u_i\right)+\lambda\left(x-f\right)^2 \tag{16}$$

where $w_i\geq0$ are the non-negative weights, u_i are neighboring values such that $u_1\leq u_2\leq\cdots\leq u_n$.

Given a pixel, a window is created around the pixel of size $[2ws+1, 2ws+1]$ where ws governs the size of the window. At the

next step, the Euclidean distance d_i is computed between this center pixel and the neighboring pixels within the window [*ws*,*ws*]. The weights are finally computed with the Gaussian as:

$$w_i = e^{-\frac{d_i^2}{2\sigma_c^2}} \tag{17}$$

where σ_c is the standard deviation which determines the degree to which nearby pixels contribute to the weighted median. The choice of these parameters will be discussed subsequently.

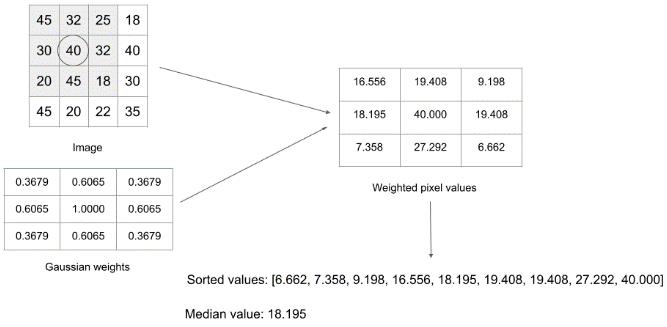

Fig.3. Demonstration of the weighted median filtering process with a specific example

4.3 RESULTS ON THE MIDDLEBURY BENCHMARK DATASETS

We evaluated the effectiveness of our flow estimation approach on selected rotational images from the middlebury dataset [16] [17] namely the *venus*, *hydrangea* and *rubberwhale* sequences. The results are shown in Fig.4.

Fig.4. Estimated flow fields for the *rubberwhale*, *hydrangea* and *venus* sequences from the middlebury dataset.

4.4 COMPARISON WITH EXISTING METHODS

To further highlight the efficiency of our model, we compare our results with some of the well-known variational optical flow models using the widely used error metrics in the literature, namely the average angular error (AAE) and the end-point error (EPE). The AAE is computed as:

$$AAE = \frac{u_c \cdot u_e}{|u_c||u_e|} \tag{18}$$

where u_c is the computed flow and u_e is the exact flow. This metric was first used by Barron et al. [6] in their pioneering work where they evaluated the performance of several existing optical flow models. The EPE is computed as:

$$EPE = |u_e - u_c| = \sqrt{\left(u_1^e - u_1^c\right)^2 + \left(u_2^e - u_2^c\right)^2} \tag{19}$$

where $\left(u_1^e, u_2^e\right)$ is the exact optical flow and $\left(u_1^c, u_2^c\right)$ is the computed optical flow.

Table.1. Comparison of the Average Angular Error (AAE) and End Point Error (EPE)

	Venus	**Rubberwhale**	**Hydrangea**
	AAE/EPE	**AAE/EPE**	**AAE/EPE**
HS+NL [8]	5.498/0.333	4.992 / 0.154	2.890 / 0.250
HS+NL+GF [15]	5.140/0.310	4.667 /0.143	2.567 / 0.430
Our Method	**3.737/0.293**	**3.324/0.108**	**2.296/0.246**

The results shown in Table.1 indicate that our method achieves the best angular and endpoint errors when compared to some of the well-known Horn and Schunck based variational models.

4.5 PARAMETER SELECTION FOR IMPROVING ACCURACY

Careful selection of parameters is essential for accurate flow estimation. We performed several numerical experiments to determine suitable parameters for flow estimation. The model parameters α and β were set to 0.9 and 0.05 respectively. Similarly, as discussed before, the values 0.4 and 0.25 for primal-dual parameters τ and σ produced good results.

A coarse-to-fine grid with depth 4 was used for experimental purposes. This can also be adaptively computed by the formula mentioned in [7]. For the number of warping iterations, we observed improvement in the flow estimates for 9 iterations depending on the weight parameters *ws* and σ_c.

The weight parameters ws and σ_c played a significant role in improving the flow accuracy. The larger the *ws*, the larger the neighborhood, and the smoother the output image. However, increasing *ws* also increases the computation time. Similarly, a smaller value for σ_c led to sharper edges and better preservation of fine details, but at the cost of reduced smoothing.

Additionally, σ_c controls the trade-off between spatial and color filtering. The larger the σ_c for a given channel, the more weight is given to pixels that are similar in color to the center pixel. The smaller the σ_c, the more weight is given to pixels that are similar in spatial proximity to the center pixel. As a result, lowering the value σ_c often makes the color-coded flow field visually lighter.

The following values for *ws* and σ_c (Table.2) were experimentally found to give the best results for the venus, rubberwhale and the hydrangea sequence:

Table.2. Choice of *ws* and σ_c for different image sequences

	ws	$\boldsymbol{\sigma_c}$
Venus	7	12
Rubberwhale	5	13
Hydrangea	9	13

Here we would like to mention that these choices of *ws* and σ_c are critical in error estimation as well as for visual enhancement. For example, for the hydrangea sequence, *ws* = 5 and σ_c = 7 led to a poor color-coded flow field visually as well as relatively higher errors.

In practice, the optimal values of *ws* and σ_c depend on the specific characteristics of the image being processed, as well as

the desired balance between smoothing and preservation of fine details.

5. CONCLUSION

In this work, we have proposed an optical flow model for accurate motion estimation for rotational image sequences. In our model we have introduced an additional constraint term with a weighted penalization of the curl of the flow. The constraint term encourages the flow to have zero curl in the regions of the image where there is no rotational motion, and allows for non-zero curl in regions where there is rotational motion.

We briefly discussed about the practical relevance of our work in other application domains like cardiac motion estimation and mentioned about a flow-driven refinement process involving the curl can indeed outperform few of the existing physics-based refinement approaches.

We employed the robust Chambolle-Pock algorithm for the numerical implementation and discussed in details the effect of parameters and primal-dual parameters on the flow convergence.

To further show the effectiveness of our model, we incorporated the sophisticated implementation tools which significantly improve the flow accuracy. The results on some rotational sequences from the middlebury benchmark datasets were shown.

Further, a detailed discussion on weighted median filtering and its effectiveness was presented. Several numerical experiments were conducted to choose optimal parameters *ws* and σ_c for the design of the weighted median filter.

We observed that in general, it is recommended to experiment with different values of *ws* and σ_c to find the combination that provides the best balance of smoothing and preservation of details for a given image sequence. Our results achieve the best average angular and end-point error when compared with some of well-known optical flow models.

REFERENCES

[1] B.K.P. Horn and B.G. Schunck, "Determining Optical Flow", *Artifical Intelligence*, Vol. 17, No. 1-3, pp. 185-203, 1981.

[2] G. Aubert, R. Deriche and P. Kornprobst, "Computing Optical Flow via Variational Techniques", *SIAM Journal on Applied Mathematics*, Vol. 60, No. 1, pp. 156-182, 1999.

[3] I. Cohen, "Nonlinear Variational Method for Optical Flow Computation", *Proceedings of the Scandinavian Conference on Image Analysis*, Vol. 1, pp. 523-534, 1993.

[4] A. Wedel, T. Pock, C. Zach, H. Bischof and D. Cremers, "*An Improved Algorithm for TV-L1 Optical Flow*", Springer, 2009.

[5] W. Hinterberger, O. Scherzer, C. Schnorr and J. Weickert, "Analysis of Optical Flow Models in the Framework of the Calculus of Variations", *Numerical Functional Analysis and Optimization*, Vol. 23, No. 1-2, pp. 69-89, 2002.

[6] N. Parikh and S. Boyd, "Proximal Algorithms", *Foundations and Trends in Optimization*, Vol. 1, No. 3, pp. 123-231, 2013.

[7] J.L. Barron, D.J. Fleet and S.S. Beauchemin, "Performance of Optical Flow Techniques", *International Journal on Computer Vision*, Vol. 12, No. 1, pp. 43-77, 1994.

[8] D. Sun, S. Roth and M.J. Black, "A Quantitative Analysis of Current Practices in Optical Flow Estimation and the Principles Behind Them", *International Journal on Computer Vision*, Vol. 106, No. 2, pp. 115-137, 2014.

[9] D. Sun, S. Roth and M.J. Black, "Secrets of Optical Flow Estimation and their Principles", *Proceedings of IEEE Computer Society Conference on Computer Vision and Pattern Recognition*, pp. 2432-2439, 2010.

[10] Y. Li and S. Osher, "A New Median Formula with Applications to PDE based Denoising", *Communications in Mathematical Sciences*, Vol. 7, No. 3, pp. 741-753, 2009.

[11] A. Chambolle and T. Pock, "A First-Order Primal-Dual Algorithm for Convex Problems with Applications to Imaging", *Journal of Mathematical Imaging and Vision*, Vol. 40, No. 1, pp. 120-145, 2011.

[12] P. Perona and J. Malik, "Scale-Space and Edge Detection using Anisotropic Diffusion", *IEEE Transactions on Pattern Analysis and Machine Intelligence*, Vol. 12, No. 7, pp. 629-639, 1990.

[13] H. Dirks, "Variational Methods for Joint Motion Estimation and Image Reconstruction", *Proceedings of IEEE Computer Society Conference on Computer Vision and Pattern Recognition*, pp. 1-12, 2015.

[14] H. Doshi and N.U. Kiran, "Nonlinear Evolutionary PDE-Based Refinement of Optical Flow", *Machine Graphics and Vision*, Vol. 30, No. 1-4, pp. 45-65, 2021.

[15] T. Brox, A. Bruhn, N. Papenberg and J. Weickert, "High Accuracy Optical Flow Estimation based on a Theory for Warping", *Proceedings of European Conference on Computer Vision*, pp. 25-36, 2004.

[16] C. Zhang, L. Ge, Z. Chen, R. Qin, M. Li and W. Liu, "Guided Filtering: Toward Edge-Preserving for Optical Flow", *IEEE Access*, Vol. 6, pp. 26958-26970, 2018.

[17] S. Baker, D. Scharstein, J.P. Lewis, S. Roth, M.J. Black and R. Szeliski, "A Database and Evaluation Methodology for Optical Flow", *International Journal on Computer Vision*, Vol. 92, No. 1, pp. 1-31, 2011.

[18] S. Baker, D. Scharstein, J.P. Lewis, S. Roth, M. Black and R. Szeliski, "Middlebury Stereo Vision Page", *International Journal on Computer Vision*, Vol. 88, No. 2, pp. 1-14, 2007.

[19] T. Liu, "OpenOpticalFlow: An Open Source Program for Extraction of Velocity Fields from Flow Visualization Images", *Journal of Open Research Software*, Vol. 5, No. 1, pp. 1-12, 2017

[20] B. Liu, B. Wang and D.S. Choi, "Flow Structures of Jupiter's Great Red Spot Extracted by using Optical Flow Method", *Physics of Fluids*, Vol. 24, pp. 1-13, 2012.

[21] L. Yin, R. Yang, M. Gabbouj and Y. Neuvo, "Weighted Median Filters: A Tutorial", *IEEE Transactions on Circuits and Systems-II, Analog and Digital Signal Processing*, Vol. 43, No. 3, pp. 1-13, 1996.